Magnetometer-Free, IMU-Based Foot Progression Angle Estimation for Real-Life Walking Conditions

Tian Tan, *Graduate Student Member, IEEE*, Zachary A. Strout, *Graduate Student Member, IEEE*, Haisheng Xia, *Member, IEEE*, Mostafa Orban, *Member, IEEE*, and Peter B. Shull, *Member, IEEE*

***Abstract*— Foot progression angle (FPA) is vital in many disease assessment and rehabilitation applications, however previous magneto-IMU-based FPA estimation algorithms can be prone to magnetic distortion and inaccuracies after walking starts and turns. This paper presents a foot-worn IMU-based FPA estimation algorithm comprised of three key components: orientation estimation, acceleration transformation, and FPA estimation via peak foot deceleration. Twelve healthy subjects performed two walking experiments to evaluation IMU algorithm performance. The first experiment aimed to validate the proposed algorithm in continuous straight walking tasks across seven FPA gait patterns (large toe-in, medium toe-in, small toe-in, normal, small toe-out, medium toe-out, and large toe-out). The second experiment was performed to evaluate the proposed FPA algorithm for steps after walking starts and turns. Results showed that FPA estimations from the IMU-based algorithm closely followed marker-based system measurements with an overall mean absolute error of 3.1±1.3 deg, and the estimation results were valid for all steps immediately after walking starts and turns. This work could enable FPA assessment in environments where magnetic distortion is present due to ferrous metal structures and electrical equipment, or in real-life walking conditions when walking starts, stops, and turns commonly occur.**

***Index Terms*— Wearable sensing, foot kinematics, gait analysis, walking starts, walking turns.**

I. Introduction

FOOT progression angle (FPA) is a critical walking gait parameter for disease assessment and rehabilitation. It is a clinical measure to assess cerebral palsy [1], [2], distal tibial physeal fractures [3], and gastrocnemius inflexibility [4]. Also, FPA modification is a potential gait rehabilitation alternative for knee osteoarthritis patients because it can reduce the peak knee adduction moment [5]–[7] and reduce knee pain [8], [9]. Additionally, FPA has a significant impact on the distribution of foot pressure during walking [10], [11], and thus a desirable pressure transfer can be achieved by adults [12] or children [13] through proper FPA modifications.

Measurement of FPA is traditionally performed with optical motion capture systems, which are expensive and confine the gait analysis within specialized laboratories. Some clinical applications such as long-term gait retraining may require continuous FPA monitoring and modification throughout the day to enhance adherence to the prescribed gait pattern [14]. Compared with optical motion capture systems, the small size and light weight of inertial measurement units (IMUs) make them a convenient and practical choice for wearable body kinematics monitoring in real-life scenarios [15].

One major problem with previous magneto-IMU-based FPA algorithm is that it relies on magnetometer outputs to estimate the foot orientation with respect to the earth [16], [17], so neither the foot heading direction nor the foot orientation during stance phase can be accurately estimated under distorted magnetic fields. Inaccuracies caused by magnetic distortion are quite common in orientation estimation studies when the experiments were performed inside of a movement analysis lab [18] or in the vicinity of ferrous materials such as mobility aid devices [19], speakers [20], and steel cases [21]. Magnetometers are particularly prone to magnetic distortion when placed on foot because of ferrous metal structures in the floor that are often in construction for reinforcement [22]. Thus, a magnetometer-free FPA estimation algorithm could significantly improve the practical implementation of IMU-based FPA estimation in real-life scenarios involving magnetic distortion.

Another problem with previous magneto-IMU-based FPA algorithms is that the foot heading direction is estimated by double integrating noisy accelerometer data, so a complementary filter is required to increase the accuracy [16]. Due to such a filter, the foot heading direction can only slowly converge to the walking direction after each walking start or turn, making the estimation results of the first roughly

Manuscript received August 20, 2020; revised October 15, 2020; accepted December 21, 2020. Date of publication December 25, 2020; date of current version March 1, 2021. This work was supported by the National Natural Science Foundation of China under Grant 51875347. *(Corresponding author: Peter B. Shull.)*

Tian Tan, Zachary A. Strout, and Peter B. Shull are with the State Key Laboratory of Mechanical System and Vibration, School of Mechanical Engineering, Shanghai Jiao Tong University, Shanghai 200240, China (e-mail: alantantian@sjtu.edu.cn; zstrout@sjtu.edu.cn; pshull@sjtu.edu.cn).

Haisheng Xia is with the Department of Automation, University of Science and Technology of China, Hefei 230026, China (e-mail: hsxia@ustc.edu.cn).

Mostafa Orban is with the Faculty of Engineering at Shoubra, School of Mechanical Engineering, Benha University, Qalyubia 13518, Egypt (e-mail: mustafa.essam@feng.bu.edu.eg).

Digital Object Identifier 10.1109/TNSRE.2020.3047402

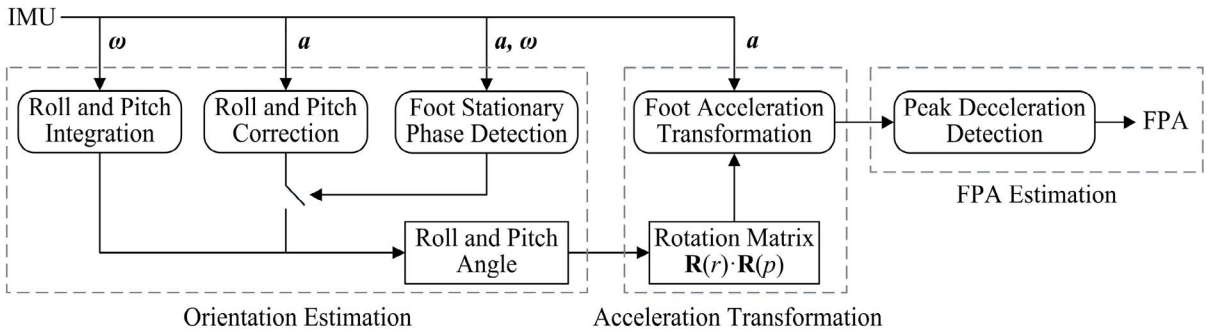

Fig. 1. Flow chart of the proposed FPA estimation algorithm. The algorithm consists of three key components: 1) orientation estimation via gyroscope integration and accelerometer correction, 2) acceleration transformation via estimated roll and pitch, and 3) FPA estimation via peak foot deceleration.

7 steps invalid. Therefore, previous magneto-IMU-based algorithm approaches may be limited in real-life walking conditions, which would typically involve many walking starts/stops and turns. Walking starts are quite common because 75% of all walking bouts are relatively short (less than 40 steps) [23]. Also, walking turns are quite common in real-life walking activities [24]. Despite the importance of walking starts and turns, an algorithm that could quickly provide valid FPA estimates after walking starts and turns has not yet been proposed.

The purpose of this paper was to present a magnetometer-free, IMU-based FPA estimation algorithm for real-life walking conditions. We hypothesized that the proposed algorithm would enable accurate estimation of the FPA for normal, toe-in, and toe-out gait patterns in continuous straight walking tasks. We also hypothesized that the proposed algorithm can more quickly provide valid FPA estimates than a magneto-IMU-based FPA algorithm for steps after walking starts and turns.

Algorithm 1 IMU-Based FPA Estimation

```
for sample i = 1 to N
    Detect foot stationary phase, heel-strike, and toe-off
    if i is in the middle of n^th step's stance phase, then
        Initialize r, p of sample i from accelerometer with (4) and (5)
        for j = i to toe-off of (n − 1)^th step
            Calculate r_gyr, p_gyr of sample j from gyroscope with (6)
            if j ∈ foot stationary phase
                Correct r, p of sample j from accelerometer with (7)
            end if
            Transform the foot acceleration with (16)
        end for
        Calculate the FPA of n^th step with (23)
    end if
end for
```

II. IMU-Based FPA Estimation Algorithm

An IMU-based FPA estimation algorithm was developed based on the following three key components (Fig. 1): 1) orientation estimation, 2) acceleration transformation, and 3) FPA estimation. First, the orientation of the foot is partially estimated based on the measured angular velocity and gravity vector. Second, the estimated orientation is converted to rotation matrix to transform the accelerometer data. Finally, the FPA of each step is estimated from the peak foot deceleration during swing phase. To help readers implement the proposed IMU-based algorithm, a pseudocode (Algorithm 1) is provided with standard programming structure.

A. Orientation Estimation

Let S_0 denote the sensor frame with alignment offset, whose orientation is determined by sensor placement. Also, let S denote the calibrated sensor frame, whose y-axis aligns with foot vector (from the calcaneus to the head of second metatarsal), z-axis aligns with the gravity vector pointing upwards when the shoe is flat on the ground, and x-axis is perpendicular to these axes following the right-hand rule. When the sensor was placed in the shoe, the orientation difference between S_0 and S was calibrated based on the spatial relationship between the calcaneus, the head of second metatarsal, and the sensor [14]. Then, a transformation matrix R_{cali} was computed and used to transform all the outputs from S_0 to S. For simplicity, the calibrated sensor frame will be referred to as sensor frame in the rest of this paper.

Let C denote a current step frame, which is updated at each foot stationary phase. Frame C's y-axis aligns with the foot heading direction (line of progression), z-axis aligns with the gravity vector, and x-axis is defined by right-hand rule. The orientation of sensor frame with respect to current step frame is:

$$\mathbf{R}_S^C = \mathbf{R}(y)\mathbf{R}(p)\mathbf{R}(r), \tag{1}$$

where the r, p, and y are Euler angles called roll, pitch, and yaw, respectively. For each step, the FPA is defined by the angle between the foot heading direction (aligns with y-axis of current step frame) and the foot vector (aligns with y-axis of sensor frame after sensor orientation calibration) at mid-stance, so the FPA is equivalent to the Euler angle yaw. To calculate yaw, we introduced a "foot flat" frame F, which is an intermediate coordinate frame defined by rotating the current step frame about its z-axis by -y deg. The orientation

relationship between sensor frame, current step frame, and foot flat frame are:

$$\mathbf{R}_S^F = \mathbf{R}(p)\mathbf{R}(r) \text{ and} \tag{2}$$

$$\mathbf{R}_F^C = \mathbf{R}(y). \tag{3}$$

An adaptive gait event detection algorithm [25] has been implemented to determine heel-strike, toe-off, and foot stationary phase based on the foot pitch angular velocity, thereby demarcating the swing and stance phase. The detection thresholds and detection intervals were adjusted after each valid step to adapt gait pattern differences [25]. For each step, starting from the mid-stance, the r and p are initialized by:

$$\begin{bmatrix} r_{acc} \\ p_{acc} \end{bmatrix}_k = \begin{bmatrix} \arctan\left(a_y^S / a_z^S\right) \\ \arctan\left(-a_x^S / \sqrt{(a_y^S)^2 + (a_z^S)^2}\right) \end{bmatrix}_k, \tag{4}$$

$$\begin{bmatrix} r \\ p \end{bmatrix}_k = \begin{bmatrix} r_{acc} \\ p_{acc} \end{bmatrix}_k, \tag{5}$$

where r_{acc} and p_{acc} denote the angles estimated from the accelerometer, a_x^S, a_y^S, and a_z^S denote accelerometer outputs, and k denotes the sample in the middle of foot stationary phase. Then, the r and p are estimated from the end to the start of the current step so that those two angles are more accurately estimated with less integration drift during the deceleration period the swing phase. For each sample j from $k-1$ to the toe-off of the last step, reversely update the r_{gyr} and p_{gyr} of sample j by gyroscope integration [26] as follows:

$$\begin{bmatrix} r_{gyr} \\ p_{gyr} \end{bmatrix}_j = \begin{bmatrix} r \\ p \end{bmatrix}_{j+1} - \begin{bmatrix} 1 & \mathrm{S}r\mathrm{S}p/\mathrm{C}p & \mathrm{C}r\mathrm{S}p/\mathrm{C}p \\ 0 & \mathrm{C}r & -\mathrm{S}r \end{bmatrix}_{j+1} \times \begin{bmatrix} \omega_x \\ \omega_y \\ \omega_z \end{bmatrix}_{j+1}, \tag{6}$$

where r_{gyr} and p_{gyr} denote the angles estimated from the gyroscope, S and C denote sin and cos functions, ω_x, ω_y, and ω_z, denote gyroscope outputs. Also, the gravity measured by the accelerometer is used to correct the gyroscope integration drift via a gradient descent algorithm [17]. This algorithm corrected r_{gyr} and p_{gyr} of sample j in the gradient direction as follows:

$$\begin{bmatrix} r \\ p \end{bmatrix}_j = \begin{bmatrix} r_{gyr} \\ p_{gyr} \end{bmatrix}_j - \beta \frac{\nabla \boldsymbol{f}}{\|\nabla \boldsymbol{f}\|}, \tag{7}$$

$$\beta = \begin{cases} \sqrt{\frac{3}{4}}\tilde{\omega}_{\max} & \text{if } j \text{ in foot stationary phase} \\ 0 & otherwise, \end{cases} \tag{8}$$

where $\boldsymbol{f}$ denotes the objective function to minimize, ∇ accent denotes the gradient direction, and β denotes the correction rate. The β is set based on the maximum gyroscope measurement error ($\tilde{\omega}_{\max}$) if the sample j belongs to foot stationary phase [16], and it is set to zero if the accelerometer outputs deviate from the gravity due to foot movement. Because gyroscope drift error can cause misalignment between the gravity vector and the accelerometer output, the objective function $\boldsymbol{f}$ is constructed to minimize alignment difference via correcting r_{gyr} and p_{gyr} as follows:

$$\min_{r_{gyr}, p_{gyr}} f\left(r_{gyr}, p_{gyr}, \hat{\boldsymbol{a}}^S, \hat{\boldsymbol{g}}^F\right), \tag{9}$$

$$f = \left[R(p_{gyr})R(r_{gyr})\right]^T \hat{\boldsymbol{g}}^F - \hat{\boldsymbol{a}}^S, \tag{10}$$

where the $\hat{}$ accent mark denotes a normalized vector of unit length, $\hat{\boldsymbol{a}}^S$ denotes the normalized accelerometer output, and $\hat{\boldsymbol{g}}^F$ denotes the normalized gravity vector. The objective function becomes (13) when substituting (11) and (12) into (10) as follows:

$$\hat{\boldsymbol{a}}^S = \left[a_x^S, a_y^S, a_z^S\right] / \left\|\boldsymbol{a}^S\right\|, \tag{11}$$

$$\hat{\boldsymbol{g}}^F = [0, 0, 1], \tag{12}$$

$$\boldsymbol{f} = \begin{bmatrix} -\mathrm{S}p_{gyr} - a_x^S / \left\|\boldsymbol{a}^S\right\| \\ \mathrm{S}r_{gyr}\mathrm{C}p_{gyr} - a_y^S / \left\|\boldsymbol{a}^S\right\| \\ \mathrm{C}r_{gyr}\mathrm{C}p_{gyr} - a_z^S / \left\|\boldsymbol{a}^S\right\| \end{bmatrix}. \tag{13}$$

Therefore, the objective function's Jacobian and its gradient direction are:

$$\boldsymbol{J} = \begin{bmatrix} 0 & -\mathrm{C}p_{gyr} \\ \mathrm{C}r_{gyr}\mathrm{C}p_{gyr} & -\mathrm{S}r_{gyr}\mathrm{S}p_{gyr} \\ -\mathrm{S}r_{gyr}\mathrm{C}p_{gyr} & -\mathrm{C}r_{gyr}\mathrm{S}p_{gyr} \end{bmatrix} \text{ and} \tag{14}$$

$$\nabla \boldsymbol{f} = \boldsymbol{J}^T \boldsymbol{f}. \tag{15}$$

Now, the r and p of sample j can be updated by substituting (13), (14), and (15) into (7).

B. Acceleration Transformation

For each sample j, the measured foot acceleration is transformed from sensor frame to foot flat frame by:

$$a^F = \mathbf{R}(p)\mathbf{R}(r)a^S, \tag{16}$$

where $\mathbf{R}(r)$ and $\mathbf{R}(p)$ are rotation matrix defined by:

$$\mathbf{R}(r) = \begin{bmatrix} 1 & 0 & 0 \\ 0 & \mathrm{C}r & -\mathrm{S}r \\ 0 & \mathrm{S}r & \mathrm{C}r \end{bmatrix}, \tag{17}$$

$$\mathbf{R}(p) = \begin{bmatrix} \mathrm{C}p & 0 & \mathrm{S}p \\ 0 & 1 & 0 \\ -\mathrm{S}p & 0 & \mathrm{C}p \end{bmatrix}. \tag{18}$$

After transformation, the foot acceleration in foot flat frame is smoothed via a 0.4s span Hanning window [27].

C. FPA Estimation

The relationship between the foot acceleration in foot flat frame and current step frame is:

$$\boldsymbol{a}^C = \mathbf{R}(y)a^F, \tag{19}$$

$$\mathbf{R}(y) = \begin{bmatrix} \mathrm{C}y & -\mathrm{S}y & 0 \\ \mathrm{S}y & \mathrm{C}y & 0 \\ 0 & 0 & 1 \end{bmatrix}. \tag{20}$$

For each step, since the y-axis of current step frame is aligned with the foot heading direction, the foot acceleration in x-axis of current step frame is zero:

$$a_x^C = 0. \tag{21}$$

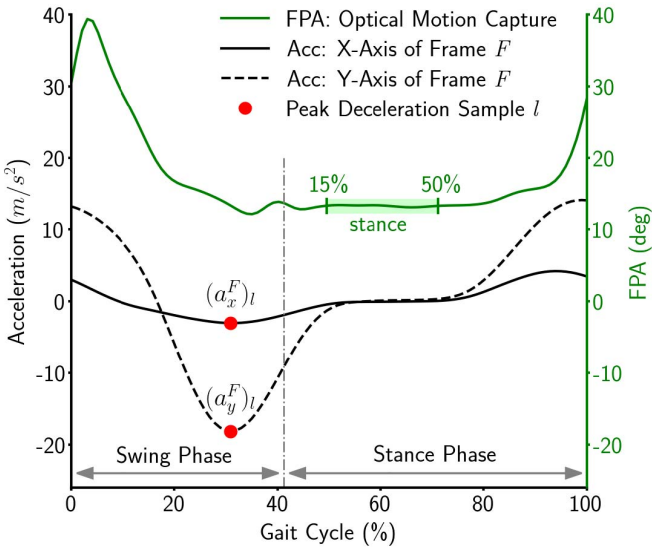

Fig. 2. A representative gait cycle showing FPA signal from optical motion capture data and foot acceleration signals from transformed IMU data (section II-B). Ground-truth FPA was computed as the average value from 15% to 50% of stance phase (the green shaded interval) [6]. The proposed algorithm estimated FPA based on peak foot deceleration (the red dots) according to (23).

The relationship between the acceleration of different axes can be obtained by substituting (21) into the first row of (19) as follows:

$$0 = \cos(y)a_x^F - \sin(y)a_y^F, \tag{22}$$

so the FPA of the current step can be estimated by:

$$FPA = y = \arctan\left[(a_x^F/a_y^F)_l\right], \tag{23}$$

where l is the sample with the largest acceleration magnitude during the second half of the swing phase (Fig. 2). This sample is selected because its signal is the strongest during the deceleration period of the swing phase.

III. Experiment I: Continuous Straight Walking

A. Experimental Testing

The first experiment was to quantify the accuracy of the proposed IMU-based algorithm in continuous straight walking tasks. Twelve healthy subjects (age: 25.8 ± 3.3; height: 1.72 ± 0.07 m; weight: 59.2 ± 8.8 kg, all male) participated in this study after giving informed consent, which was reviewed and approved by the university ethics committee (ml2018022). Three reflective markers were placed on the left shoe above the calcaneus, the head of second metatarsal, and the head of fifth metatarsal, and a motion capture system (Vicon, Oxford Metrics Group, Oxford, UK) was used to collect their trajectories at 100 Hz. Synchronized ground reaction force was measured using an instrumented treadmill (Bertec Corp., Worthington, OH, USA) at 100 Hz. Additionally, a magneto-IMU (three-axis accelerometer, three-axis gyroscope, three-axis magnetometer) was embedded in the sole of each subject's left shoe to collect inertial data and magnetic data at 100 Hz (Fig. 3) [14]. Note that the proposed algorithm only used IMU measurements for FPA estimation.

Fig. 3. Subject instrumentation layout. Reflective markers were placed on the left shoe above the calcaneus, the head of second metatarsal, and the head of fifth metatarsal. A magneto-IMU sensor was embedded in the sole of the left shoe.

Subjects performed seven walking trials (large toe-in, medium toe-in, small toe-in, normal, small toe-out, medium toe-out, and large toe-out) at self-selected speeds (1.16 ± 0.06 m/s) on the treadmill. Prior to each trial, subjects placed their left heel on the ground and swung their left toe externally three times to collect data for synchronization (the synchronization method is described in section III-B). The trial sequence was randomized for each subject. Each trial lasted two minutes and subjects were given one minute to rest after each trial if requested. Prior to the formal experiment, subjects tried different FPA modifications and were instructed to walk with the largest modification they could comfortably maintain in large toe-in/toe-out trials. In medium and small toe-in/toe-out trials, subjects' FPA modifications were instructed to be half and a quarter as much as the largest modification, respectively.

B. Data Analysis

Marker trajectories were low-pass filtered at 15 Hz and force plate data at 50 Hz using a zero-lag second-order Butterworth filter [16]. The ground-truth stance phase was detected by the measured vertical ground reaction force with a threshold of 20 N [28]. FPA was defined by the angle between the line from the calcaneus to the head of second metatarsal and the long edge of the treadmill and was computed as the average value from 15% to 50% of stance phase (Fig. 2) [6]. FPA was considered positive when the second metatarsal head was lateral of the calcaneus. The three toe swings prior to each

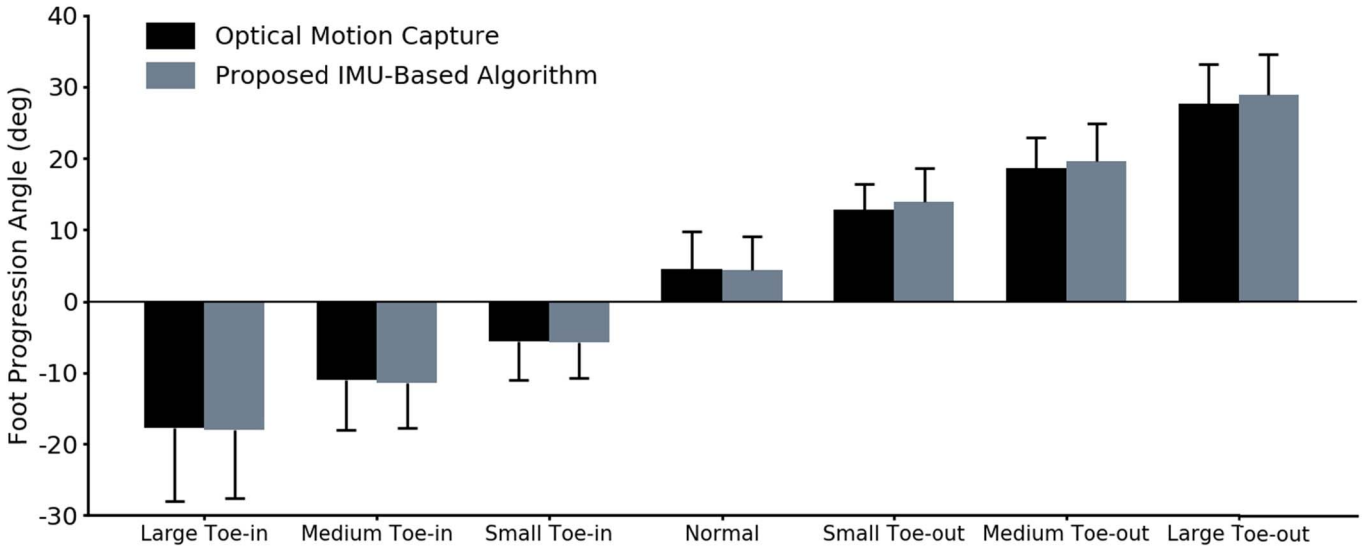

Fig. 4. Average FPA grouped by gait patterns. There was no significant difference between FPA: Optical Motion Capture and FPA: Proposed IMU-Based Algorithm for any gait pattern (p values were 0.94, 0.95, 0.90, 0.94, 0.59, 0.65, 0.62 for large toe-in, medium toe-in, small toe-in, normal, small toe-out, medium toe-out, and large toe-out gait).

trial correspond to three Euler angle yaw (orientation of sensor frame S with respect to current step frame C) peaks. The peaks computed from the magneto-IMU data and the peaks measured by the motion capture system were matched manually to synchronize the data. For each trial, 50 steps after the first 20 steps were used for analysis. A paired t-test was used to determine if there were significant differences between FPA estimated by the proposed algorithm and ground-truth FPA for all seven different gait patterns. The level of significance was set to 0.05.

C. Results

FPA estimated by the proposed algorithm closely matched ground-truth FPA for all seven gait patterns (Fig. 4). The overall mean absolute error, mean error, and Pearson's correlation coefficient across all walking gait patterns were 3.1 ± 1.3 deg, 0.3 ± 2.7 deg, and 0.99 ± 0.0, respectively. The mean error was substantially smaller than the mean absolute error because positive and negative errors were cancelled out in mean error computation. The mean absolute error for large toe-in, medium toe-in, small toe-in, normal, small toe-out, medium toe-out, and large toe-out trial were 2.7 ± 1.2 deg, 2.7 ± 1.4 deg, 2.5 ± 1.0 deg, 2.6 ± 1.1 deg, 3.8 ± 2.4 deg, 3.8 ± 2.5 deg, 4.0 ± 2.1 deg, respectively. There was no significant difference between FPA estimated by the proposed algorithm and ground-truth FPA for any of the seven gait patterns (Fig. 4). Estimated FPA from the foot-worn IMU and measured FPA from the optical motion capture system for each step of a representative subject also demonstrated high correlation between the proposed algorithm estimations and ground-truth FPA (Fig. 5).

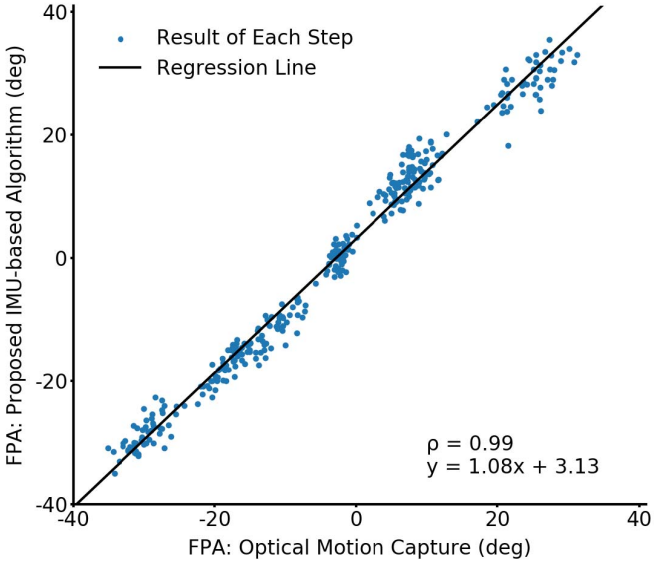

Fig. 5. Scatter plot and linear regression line showing FPA estimation results of a representative subject. The mean absolute error, mean error, and correlation coefficient of this subject were 3.2 deg, 2.8 deg, and 0.99, respectively.

IV. Experiment II: Walking Starts and Turns

A. Experimental Testing

The second experiment was to test whether the proposed IMU-based algorithm can more quickly provide valid FPA estimates compared with a magneto-IMU-based algorithm for steps after walking starts and turns. Twelve healthy subjects (age: 24.5 ± 1.8; height: 1.77 ± 0.04 m; weight: 70.2 ± 8.8 kg, all male) participated in this study after giving informed consent, which was reviewed and approved by the university ethics committee (ml2018022). This experiment was performed outdoors because the laboratory walkway was not long enough to accommodate required walking distances. The same magneto-IMU from the continuous straight walking experiment was embedded in the sole of each subject's left shoe to collect inertial data and magnetic data at 100 Hz. Note that the proposed algorithm only used inertial data for FPA estimation, and the magnetic data were collected for the magneto-IMU-based algorithm.

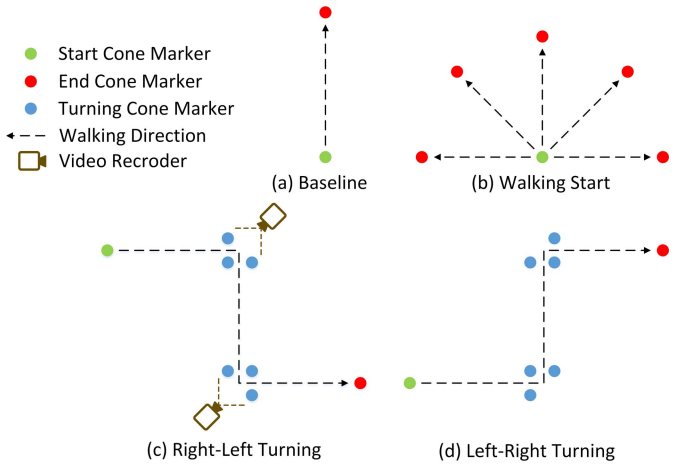

Fig. 6. Sketch map of (a) baseline, (b) walking start, (c) right-left turning, and (d) left-right turning trials. For all trials, subjects walked from start cone markers (green dots) towards end cone markers (red dots) along the dashed arrow. For turning trials, cone marker sets (blue dots) were placed in shapes of isosceles right triangles to indicate turn direction.

Prior to the formal testing, subjects tried baseline trial, walking start trial, and turning trial for one time. Afterwards, they performed a baseline trial (Fig. 6(a)), where they walked naturally and straightly from the start cone marker towards the end cone marker. The two cone markers were placed far enough to accommodate at least 25 ipsilateral steps. Then subjects performed ten walking start trials and ten turning trials with a randomized sequence. For walking start trials, subjects walked naturally and straightly from the start cone marker towards each end cone marker (placed at left, left-forward, forward, right-forward, and right direction) twice with a randomized sequence (Fig. 6(b)). The start and end cone markers were placed far enough to accommodate at least 20 ipsilateral steps. The ten turning trials consist of five right-left turning trials (Fig. 6(c)) and five left-right turning trials (Fig. 6(d)) with a randomized sequence. For each turning trial, subjects walked naturally and straightly from the start cone marker towards the first cone marker set and turned 90 degrees to right/left when passing the first cone marker set. Then, they continued walking without stopping towards the second cone marker set, turned 90 degrees to left/right when passing the second cone marker set, and continued walking towards the end cone marker. The distances from the start cone marker to the first cone marker set, from the first to the second cone marker set, and from the second cone marker set to the end cone marker were all far enough to accommodate at least 20 ipsilateral steps. Each cone marker set was placed in a shape of an isosceles right triangle with 1.5 m side lengths. For right-left trials, two video recorders were placed behind the hypotenuse of the first and the second marker set to record the right and left turns, respectively (Fig. 6(c)).

B. Data Analysis

For the baseline trial, 10 steps after the first 15 steps were used to calculate the mean and the standard deviation (SD) of baseline FPA. The ±3SD of baseline FPA obtained from the magneto-IMU-based algorithm was used as the criterion to determine valid FPA estimations. Also, to visually demonstrate this criterion and compared it to different subjects' data with different baseline FPAs for walking start and turning trials, each subject's baseline FPA obtained from IMU-based/magneto-IMU-based algorithm was subtracted from the FPA estimated by IMU-based/magneto-IMU-based algorithm. Therefore, after subtraction, correct FPA estimations are expected to fluctuate around zero for straight walking steps. For each walking start trial, FPA of the first 8 left steps estimated by both two algorithms were analyzed to determine if they were within the ±3SD of baseline FPA. For each turning trial, the step with the largest positive foot heading direction change (calculated by integration of gyroscope z-axis output) was determined as one left turning step, and one of its adjacent step with the larger heading direction change was determined as the other left turning step. Similarly, the step with the largest negative heading direction change and one of its adjacent step were determined as two right turning steps. Then, the first 8 steps after both left and right turning steps were analyzed together to determine if they were within the ±3SD of baseline FPA. Additionally, a single investigator analyzed videos of all the right-left turning trials to count the number of turning steps, which were identified if there is a change in the left foot's heading direction before heel-strike [24].

C. Results

The 3SD of baseline FPA was 7.0 deg. FPA estimated by the proposed IMU-based algorithm was valid (within ±3SD of baseline FPA) for all steps immediately after walking starts and turns, while FPA estimated by the magneto-IMU-based algorithm were invalid for the first 6 and 7 steps after walking starts and turns, respectively (Fig. 7). Also, according to the videos, the average number of left steps identified in each turn was 2.01 ± 0.35 steps, and the percentage of one, two, and three steps were 5.8%, 87.5%, and 6.7%, respectively.

V. Discussion

This paper presented an IMU-based FPA estimation algorithm for real-life walking conditions. In support of our first hypothesis, FPA estimated by the proposed IMU-based algorithm closely matched ground-truth FPA for normal, toe-in, and toe-out gait patterns in continuous straight walking tasks. In support of our second hypothesis, the proposed IMU-based algorithm can provide valid FPA estimation for all steps immediately after walking starts and turns.

Previous magneto-IMU-based FPA algorithm is accurate for continuous straight walking tasks in environments free of magnetic distortion, so it directly enabled a few studies including sensorized shoes for outdoor over-ground FPA monitoring [14], [29] and haptic feedback-sensorized shoes for FPA modification [30]. However, that algorithm relied on the magnetometer data for orientation correction, so it is prone to magnetic distortion. Also, that algorithm utilized double integration of noisy accelerometer data, so it requires a complementary filter to suppress the noise via fusion of the current step estimation with previous step estimations. Despite its high

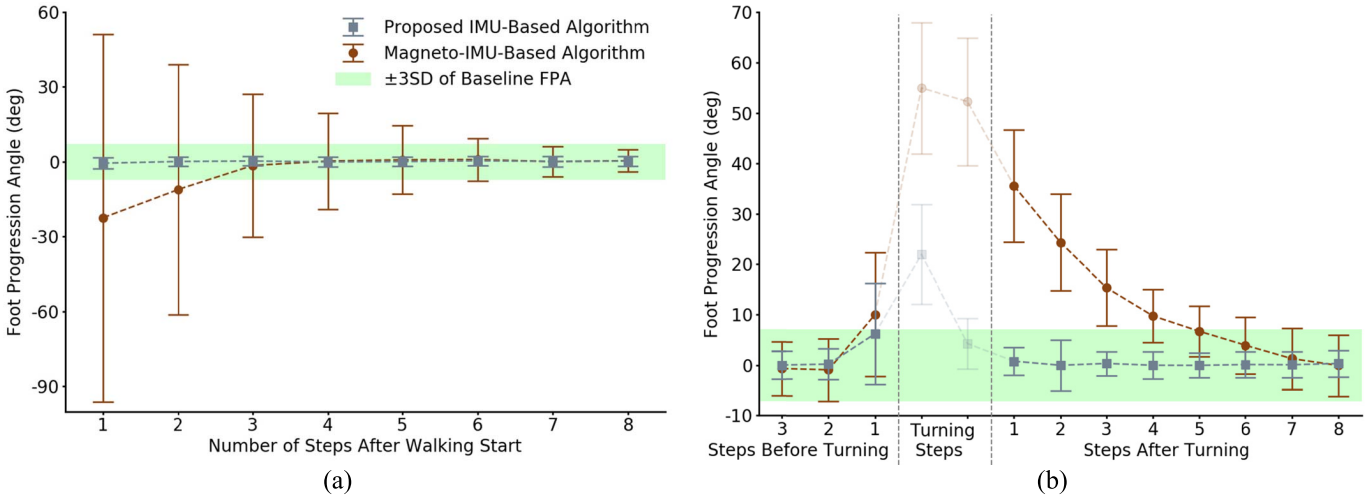

Fig. 7. Mean with one standard deviation of the FPA estimated by the proposed IMU-based algorithm and magneto-IMU-based algorithm for (a) the first 8 steps after walking starts and (b) steps before, during, and after 90-degree walking turns. The mean baseline FPA was subtracted from FPA estimations to remove the baseline FPA differences between subjects. The green shaded area represents the ±3SD of baseline FPA. Turning step results were plotted lightly to emphasize that the FPA is not well defined when the heading direction is changing [30].

accuracy in continuous straight walking tasks, that algorithm updates slowly after walking starts and turns, making the FPA estimation of the first 6-7 step invalid (Fig. 7). On the contrary, the proposed magnetometer-free, IMU-based FPA algorithm utilized the peak foot deceleration during the swing phase, and no complementary filter was required to suppress the noise, so the estimation of each step is independent of its previous steps. Despite its relatively lower accuracy in continuous straight walking tasks, the proposed IMU-based algorithm performed substantially better than previous magneto-IMU-based algorithm for steps after walking starts and turns (Fig. 7).

The mean absolute error, mean error, and correlation coefficient of the proposed IMU-based algorithm were 3.2 deg, 0.3 deg, and 0.99, which were comparable with that reported by other wearable foot orientation estimation studies. Karatsidis *et al.* [31] used a set of seven magneto-IMUs and the lower body kinematics reconstructed by commercial software to estimate FPA, and the root mean square error were between 1.9 and 2.6 deg. However, this method is based on closed-source software, and the placement of seven IMUs on various body segments is inconvenient. Young *et al.* [32] used a chest-worn camera and a "visual feature matching" method to estimate FPA, and the mean error was 0.15 deg. However, the validation experiment only involved a normal gait pattern, and strapping a camera in front of the chest is inconvenient for real-life FPA monitoring. Rouhani *et al.* [33] used four IMUs to estimate the orientation difference between foot and ankle, and the mean correlation coefficient was 0.93. Mariani *et al.* [34] used a foot-worn IMU to estimate the foot heading direction change, and the mean error was 1.6 ± 6.1 deg. Bidabadi *et al.* [35] used a foot-worn IMU to estimate foot pitch angle (rotation in sagittal plane), and the correlation coefficient was 0.98.

The proposed algorithm estimated the FPA based on the peak foot deceleration measured before heel-strike, so theoretically the estimation can be finished immediately after mid-stance. Therefore, this algorithm can potentially enable FPA feedback during the second half of stance phase, which is an important prerequisite for real-time FPA modification research [5], [36], [37]. A different FPA estimation strategy can be based on the peak foot acceleration during the first half of swing phase, but this strategy requires IMU data captured after toe-off for estimation, making the real-time FPA feedback infeasible. Also, the accuracy of the latter strategy might be lower because the foot orientation change after toe-off is relatively larger than that before heel-strike [38].

When the foot heading direction is changing, the FPA is not well defined [30], so the results of turning steps were plotted lightly (Fig. 7(b)). Two turning steps were identified from each turning trial because the average number of turning steps was 2.01. The FPA estimation of the last step before turning was invalid (Fig. 7(b)), which might be because some subjects performed walking turns with three steps in a few trials, or because the proposed algorithm made an invalid FPA estimation before turning.

One limitation of this study is that no experiment was performed to validate the immunity of the proposed magnetometer-free, IMU-based FPA algorithm to magnetic distortion. Future studies should investigate the precise influence of various magnetic distortion on the proposed algorithm and other FPA algorithms. Another limitation is that results of the second experiment was not validated via our optical motion capture system due to inadequate camera view distance. Future studies may evaluate the proposed algorithm for steps after walking starts/turns across various toe-in/toe-out gaits using motion capture cameras with adequate view distance.

VI. Conclusion

The proposed IMU-based algorithm provides comparable FPA estimation accuracy during continuous straight walking and higher validity after walking starts and turns compared with a magneto-IMU-based algorithm. This magnetometer-free algorithm could enable FPA estimation in environments where magnetic distortion is present due

to ferrous metal structures and electrical equipment. This algorithm could also enable more accurate FPA monitoring in real-life walking conditions when walking starts, stops, and turns commonly occur.

REFERENCES

[1] S. A. Rethlefsen, B. S. Healy, T. A. L. Wren, D. L. Skaggs, and R. M. Kay, "Causes of intoeing gait in children with cerebral palsy," *J. Bone Joint Surg.-Amer. Volume*, vol. 88, no. 10, pp. 2175–2180, Oct. 2006.

[2] L. A. Cao, S. A. Rethlefsen, T. A. L. Wren, and R. M. Kay, "Causes of out-toeing gait in children with cerebral palsy," *Gait Posture*, vol. 76, pp. 141–145, Feb. 2020.

[3] V. C. Phan, E. Wroten, and D. A. Yngve, "Foot progression angle after distal tibial physeal fractures," *J. Pediatric Orthopaedics*, vol. 22, no. 1, pp. 31–35, Jan. 2002.

[4] S.-K. Wu, S.-Z. Lou, H.-M. Lee, H.-Y. Chen, and J.-Y. You, "Gastrocnemius inflexibility on foot progression angle and ankle kinetics during walking," *Clin. Biomech.*, vol. 29, no. 5, pp. 556–563, May 2014.

[5] P. B. Shull *et al.*, "Toe-in gait reduces the first peak knee adduction moment in patients with medial compartment knee osteoarthritis," *J. Biomech.*, vol. 46, no. 1, pp. 122–128, Jan. 2013.

[6] M. Simic, T. V. Wrigley, R. S. Hinman, M. A. Hunt, and K. L. Bennell, "Altering foot progression angle in people with medial knee osteoarthritis: The effects of varying toe-in and toe-out angles are mediated by pain and malalignment," *Osteoarthritis Cartilage*, vol. 21, no. 9, pp. 1272–1280, Sep. 2013.

[7] S. Bennour, B. Ulrich, T. Legrand, B. Jolles, and J. Favre, "Effects of foot progression angle on knee biomechanics during gait modification," *Comput. Methods Biomech. Biomed. Eng.*, vol. 20, pp. 17–18, Oct. 2017.

[8] P. B. Shull *et al.*, "Six-week gait retraining program reduces knee adduction moment, reduces pain, and improves function for individuals with medial compartment knee osteoarthritis," *J. Orthopaedic Res.*, vol. 31, no. 7, pp. 1020–1025, Jul. 2013.

[9] M. A. Hunt and J. Takacs, "Effects of a 10-week toe-out gait modification intervention in people with medial knee osteoarthritis: A pilot, feasibility study," *Osteoarthritis Cartilage*, vol. 22, no. 7, pp. 904–911, Jul. 2014.

[10] M. K. Hastings, J. R. Gelber, E. J. Isaac, K. L. Bohnert, M. J. Strube, and D. R. Sinacore, "Foot progression angle and medial loading in individuals with diabetes mellitus, peripheral neuropathy, and a foot ulcer," *Gait Posture*, vol. 32, no. 2, pp. 237–241, Jun. 2010.

[11] Y.-C. Lai, H.-S. Lin, H.-F. Pan, W.-N. Chang, C.-J. Hsu, and J.-H. Renn, "Impact of foot progression angle on the distribution of plantar pressure in normal children," *Clin. Biomech.*, vol. 29, no. 2, pp. 196–200, Feb. 2014.

[12] D. Rosenbaum, "Foot loading patterns can be changed by deliberately walking with in-toeing or out-toeing gait modifications," *Gait Posture*, vol. 38, no. 4, pp. 1067–1069, Sep. 2013.

[13] W.-N. Chang, A. I. Tsirikos, F. Miller, J. Schuyler, and J. Glutting, "Impact of changing foot progression angle on foot pressure measurement in children with neuromuscular diseases," *Gait Posture*, vol. 20, no. 1, pp. 14–19, Aug. 2004.

[14] H. Xia, J. Xu, J. Wang, M. A. Hunt, and P. B. Shull, "Validation of a smart shoe for estimating foot progression angle during walking gait," *J. Biomech.*, vol. 61, pp. 193–198, Aug. 2017.

[15] P. B. Shull, W. Jirattigalachote, M. A. Hunt, M. R. Cutkosky, and S. L. Delp, "Quantified self and human movement: A review on the clinical impact of wearable sensing and feedback for gait analysis and intervention," *Gait Posture*, vol. 40, no. 1, pp. 11–19, May 2014.

[16] Y. Huang, W. Jirattigalachote, M. R. Cutkosky, X. Zhu, and P. B. Shull, "Novel foot progression angle algorithm estimation via foot-worn, magneto-inertial sensing," *IEEE Trans. Biomed. Eng.*, vol. 63, no. 11, pp. 2278–2285, Nov. 2016.

[17] S. O. H. Madgwick, A. J. L. Harrison, and R. Vaidyanathan, "Estimation of IMU and MARG orientation using a gradient descent algorithm," in *Proc. IEEE Int. Conf. Rehabil. Robot.*, Jun. 2011, pp. 1–7.

[18] E. Palermo, S. Rossi, F. Patanè, and P. Cappa, "Experimental evaluation of indoor magnetic distortion effects on gait analysis performed with wearable inertial sensors," *Physiological Meas.*, vol. 35, no. 3, pp. 399–415, Mar. 2014.

[19] C. Kendell and E. D. Lemaire, "Effect of mobility devices on orientation sensors that contain magnetometers," *J. Rehabil. Res. Devices*, vol. 46, no. 7, pp. 957–962, 2009.

[20] N. Yadav and C. Bleakley, "Accurate orientation estimation using AHRS under conditions of magnetic distortion," *Sensors*, vol. 14, no. 11, pp. 20008–20024, Oct. 2014.

[21] D. Roetenberg, C. T. M. Baten, and P. H. Veltink, "Estimating body segment orientation by applying inertial and magnetic sensing near ferromagnetic materials," *IEEE Trans. Neural Syst. Rehabil. Eng.*, vol. 15, no. 3, pp. 469–471, Sep. 2007.

[22] W. H. K. de Vries, H. E. J. Veeger, C. T. M. Baten, and F. C. T. van der Helm, "Magnetic distortion in motion labs, implications for validating inertial magnetic sensors," *Gait Posture*, vol. 29, no. 4, pp. 535–541, Jun. 2009.

[23] M. S. Orendurff, "How humans walk: Bout duration, steps per bout, and rest duration," *J. Rehabil. Res. Develop.*, vol. 45, no. 7, pp. 1077–1090, Dec. 2008.

[24] B. C. Glaister, G. C. Bernatz, G. K. Klute, and M. S. Orendurff, "Video task analysis of turning during activities of daily living," *Gait Posture*, vol. 25, no. 2, pp. 289–294, Feb. 2007.

[25] P. Félix, J. Figueiredo, C. P. Santos, and J. C. Moreno, "Adaptive real-time tool for human gait event detection using a wearable gyroscope," in *Proc. Hum.-Centric Robot.*, Oct. 2017, pp. 1–9.

[26] E. Foxlin, "Inertial head-tracker sensor fusion by a complementary separate-bias Kalman filter," in *Proc. IEEE Virtual Reality Annu. Int. Symp.*, Mar. 1996, pp. 185–194.

[27] P. Podder, T. Z. Khan, M. H. Khan, and M. M. Rahman, "Comparative performance analysis of Hamming, Hanning and blackman window," *Int. J. Comput. Appl.*, vol. 96, no. 18, pp. 1–7, Jun. 2014.

[28] G. Pacini Panebianco, M. C. Bisi, R. Stagni, and S. Fantozzi, "Analysis of the performance of 17 algorithms from a systematic review: Influence of sensor position, analysed variable and computational approach in gait timing estimation from IMU measurements," *Gait Posture*, vol. 66, pp. 76–82, Oct. 2018.

[29] J. M. Charlton, H. Xia, P. B. Shull, and M. A. Hunt, "Validity and reliability of a shoe-embedded sensor module for measuring foot progression angle during over-ground walking," *J. Biomech.*, vol. 89, pp. 123–127, May 2019.

[30] H. Xia, J. M. Charlton, P. B. Shull, and M. A. Hunt, "Portable, automated foot progression angle gait modification via a proof-of-concept haptic feedback-sensorized shoe," *J. Biomech.*, vol. 107, Jun. 2020, Art. no. 109789.

[31] A. Karatsidis *et al.*, "Validation of wearable visual feedback for retraining foot progression angle using inertial sensors and an augmented reality headset," *J. NeuroEngineering Rehabil.*, vol. 15, no. 1, p. 78, Dec. 2018.

[32] J. Young, M. Simic, and M. Simic, "A novel foot progression angle detection method," in *Computer Vision in Control Systems-4* (Intelligent Systems Reference Library), vol. 136, M. N. Favorskaya and L. C. Jain, Eds. Springer, 2018, pp. 299–317, doi: 10.1007/978-3-319-67994-5_11.

[33] H. Rouhani, J. Favre, X. Crevoisier, and K. Aminian, "Measurement of multi-segment foot joint angles during gait using a wearable system," *J. Biomech. Eng.*, vol. 134, no. 6, pp. 1–8, Jun. 2012.

[34] B. Mariani, C. Hoskovec, S. Rochat, C. Büla, J. Penders, and K. Aminian, "3D gait assessment in young and elderly subjects using foot-worn inertial sensors," *J. Biomech.*, vol. 43, no. 15, pp. 2999–3006, Nov. 2010.

[35] S. Sharif Bidabadi, I. Murray, and G. Y. F. Lee, "Validation of foot pitch angle estimation using inertial measurement unit against marker-based optical 3D motion capture system," *Biomed. Eng. Lett.*, vol. 8, no. 3, pp. 283–290, Aug. 2018.

[36] B. Lindsey, O. Eddo, S. V. Caswell, M. Prebble, and N. Cortes, "Reductions in peak knee abduction moment in three previously studied gait modification strategies," *Knee*, vol. 27, no. 1, pp. 102–110, Jan. 2020.

[37] R. Richards, J. C. van den Noort, J. Dekker, and J. Harlaar, "Gait retraining with real-time biofeedback to reduce knee adduction moment: Systematic review of effects and methods used," *Arch. Phys. Med. Rehabil.*, vol. 98, no. 1, pp. 137–150, Jan. 2017.

[38] B. F. Mentiplay, M. Banky, R. A. Clark, M. B. Kahn, and G. Williams, "Lower limb angular velocity during walking at various speeds," *Gait Posture*, vol. 65, pp. 190–196, Sep. 2018.